Nutrient distribution mapping model of the Bera River basin in Saleh Bay, West Nusa Tenggara

Amar Malikal Rahman[1], *Syamsul Bahri* Agus[2*], *Taslim* Arifin[3], and *I Wayan* Nurjaya[1]

[1]Department of Marine Science, Faculty of Fisheries and Marine Science, Post-Graduate School, IPB University, IPB Dramaga Campus, Bogor 16680, Indonesia
[2]Department of Marine Technology, Faculty of Fisheries and Marine Science, Post-Graduate School, IPB University, IPB Dramaga Campus, Bogor 16680, Indonesia
[3]National Research and Innovation Agency (BRIN), KST Soekarno, Cibinong, Bogor 16911, Indonesia

Abstract. Saleh Bay is a semi-enclosed marine ecosystem that is vulnerable to nutrient inputs from surrounding watersheds. This study aimed to map the spatial distribution of watershed-derived nutrients and assess their implications for coastal water quality using numerical modeling. Simulations incorporated wind, tides, bathymetry, river discharge, and in-situ concentrations of dissolved oxygen (DO), nitrate (NO_3), ammonia (NH_4), and phosphate (PO_4). Hydrodynamic model validation against the current Copernicus Marine Service data showed strong performance, with RMSE values of 0.0316–0.0340 and correlation coefficients exceeding 0.97. Nutrient simulations indicated generally low NH_4 (<0.003 mg/L) and PO_4 (<0.010 mg/L) concentrations, with localized coastal increases of up to 0.005 mg/L for NH_4 and ≥0.014 mg/L for PO_4. NO_3 concentrations were relatively higher, ranging from <0.03 mg/L offshore to >0.055 mg/L near the Bera River mouth. DO concentrations decreased to below 3 mg/L in the southern coastal areas during the low tide. Although direct nutrient validation is limited by field data availability, the validated hydrodynamic model provides a reliable basis for nutrient transport simulations. These results highlight the dominant role of tidal dynamics and watershed inputs, and demonstrate the usefulness of numerical modeling for sustainable coastal water quality management.

Keywords: Coastal water quality, nutrient distribution, nutrient modelling, Saleh Bay, watershed inputs

1 Introduction

Saleh Bay, located northeast of Sumbawa Island, West Nusa Tenggara, is a semi-enclosed water body connected to the Flores Sea. The bay is ecologically important because of its high biodiversity, particularly in coral reef ecosystems [1]. However, increasing human activity in

* Corresponding author: sba_cacul@apps.ipb.ac.id

the surrounding watersheds threatens its sustainability through inputs of sediments, nutrients, pesticides, and other pollutants [2, 3]. These inputs contribute to water quality degradation, eutrophication, and coral reef decline [4].

Key stressors are nutrient enrichment and organic pollution. Elevated nitrate and phosphate levels, primarily from agriculture, domestic waste, and detergents, are the main drivers of eutrophication, while dissolved oxygen (DO) serves as a critical indicator of the organic load in aquatic system [5-7]. The Bera watershed, which drains into Saleh Bay, plays a major role in transporting these pollutants and thus directly influences the ecological conditions of the bay [8, 9].

Numerical modelling provides an effective approach for analyzing interactions between hydrodynamic processes and coastal water quality, particularly for assessing the transport and distribution of nutrients and pollutants that influence ecosystem health [10, 11]. Nutrient enrichment in coastal waters, especially nitrate (NO_3), ammonia (NH_3), and phosphate (PO_4), is widely recognized as a key driver of eutrophication, leading to harmful algal blooms, hypoxia, and degradation of coral reef ecosystems [5, 7, 12]. In tropical coastal systems, strong land–sea interactions combined with high rainfall further intensify the delivery of land-derived nutrients into semi-enclosed bays, accelerating water quality deterioration and altering biogeochemical processes [13].

Despite the ecological importance of Saleh Bay and the increasing anthropogenic pressure from surrounding watersheds, integrated numerical modelling of the nutrient distribution in this area remains limited. Most previous studies have focused on hydrodynamic characteristics or observational assessments without explicitly coupling validated hydrodynamic models with nutrient transport and transformation processes [14]. In contrast, studies on other tropical and semi-enclosed coastal systems have demonstrated that coupling hydrodynamic circulation with nutrient and biogeochemical modules provides critical insights into nutrient pathways, accumulation zones, and potential hypoxia risks [2, 11]. Therefore, this study addresses a clear research gap by applying a validated MIKE 21 hydrodynamic–Ecolab framework to simulate nutrient distribution from the Bera Watershed into Saleh Bay, thereby supporting evidence-based coastal water quality management.

2 Study area

This study was conducted in the Bera Watershed, Saleh Bay, West Nusa Tenggara, as shown in **Fig. 1**. Field data collection was carried out by a BRIN research team in 2024, including water sampling and field surveys to characterize the research station locations. The collected field data were subsequently processed and analyzed in April and September, representing the First and Second Transitional Seasons, respectively.

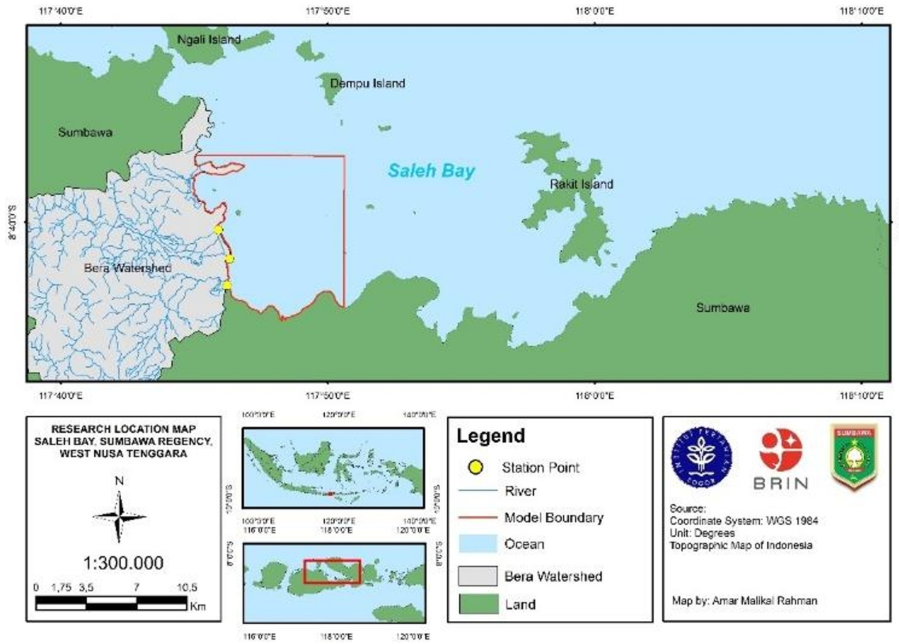

Fig. 1. Research map location, Bera Watershed, Saleh Bay, NTB.

3 Data and methods

3.1 Tools and materials

The tools used in this research included a laptop as the main hardware, ArcGIS software for map production and spatial data processing, WRPlot software for generating wind roses, and MIKE 21 software for modelling current patterns and nutrient distribution from the watershed. Microsoft Excel was used for sorting and filtering the data.

Table 1. Research data.

No	Parameter	Data source
1	Wind	ECMWF (https://www.ecmwf.int/)
2	Tide	BIG Station (https://srgi.big.go.id//)
3	Bathymetry	BATNAS (https://tanahair.indonesia.go.id/batnas)
4	Water discharge	GloFAS (https://global-flood.emergency.copernicus.eu/)
5	Nutrient Concentration	BRIN In-Situ Data 2024
6	Current	Marine Copernicus (https://data.marine.copernicus.eu/)

3.2 Data processing and analysis procedures

This study employed a coupled hydrodynamic–water quality modelling framework to simulate nutrient distribution in Saleh Bay using secondary data on wind, tides, bathymetry, river discharge, and nutrient concentrations. Tidal circulation was simulated with the hydrodynamic model, while nutrient transport and transformation of DO, NO_3, NH_4, and PO_4

were resolved using the Ecolab module. Model performance was evaluated against available observations using RMSE, and the validated outputs were analyzed to identify spatial–temporal nutrient patterns and accumulation zones, as summarized in **Fig. 2**.

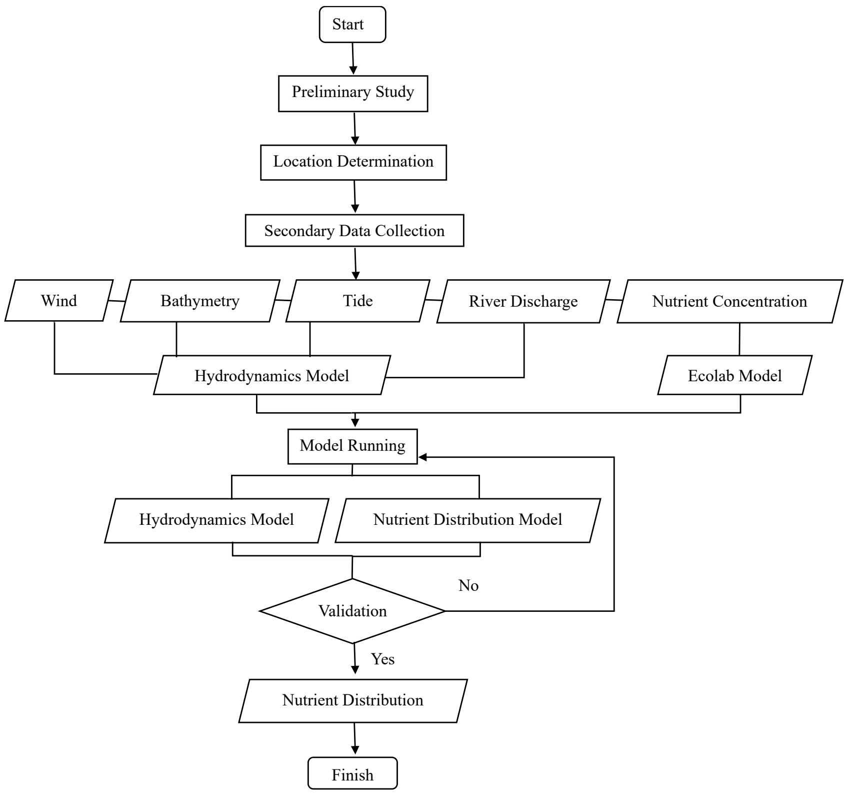

Fig. 2. Research flowchart.

3.2.1 Bathymetry

Bathymetric data were obtained from the National Bathymetry Database (BATNAS) with a spatial resolution of 6 arcsec (~ 180 m). The dataset was cropped to the model domain and used to represent the seabed topography within the MIKE 21 model, providing essential input for simulating the hydrodynamic circulation and nutrient transport in Saleh Bay.

3.2.2 Wind

Bathymetric data were obtained from the National Bathymetry Database (BATNAS) with a spatial resolution of 6 arcsec (~ 180 m). The dataset was cropped to the model domain and used to represent the seabed topography within the MIKE 21 model, providing essential input for simulating the hydrodynamic circulation and nutrient transport in Saleh Bay.

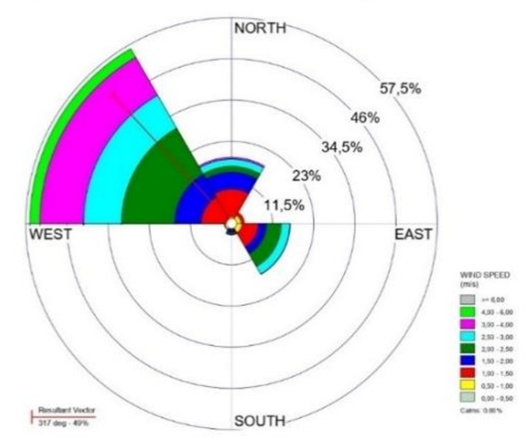

Fig. 3. Wind patterns in Saleh Bay in April 2024.

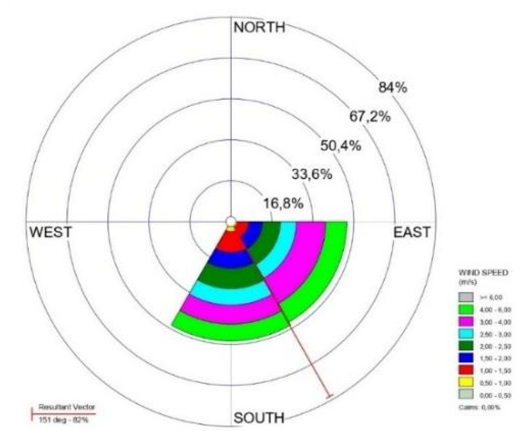

Fig. 4. Wind patterns in Saleh Bay in September 2024.

3.2.3 Tides

Tidal data were obtained from the Calabai Tidal Observation Station, provided by the Geospatial Information Agency (BIG). A 30-day sea-level dataset was analyzed using harmonic analysis to determine the main tidal constituents (M2, S2, K1, and O1). The Formzahl number was calculated to classify the tidal type, which was identified as a mixed tide with predominantly diurnal characteristics. The tidal elevation data were subsequently used as open-boundary forcing in the hydrodynamic model.

$$F = \frac{K1+O1}{M2+S2} \quad (1)$$

F : Formzahl Number
$K1$: The main single tidal element caused by solar forces.
$O1$: The main single tidal element caused by the gravitational pull of the Moon
$M2$: Main double tidal element caused by lunar force
$S2$: Main double-tidal element caused by solar force

Table 2. Tidal types based on the Formzahl number (F) [15].

Formzahl Number (F)	Tidal Type
$F \leq 0.25$	Double Tide
$0.25 < \leq 1.5F$	Mixed Tides Tend to Double
$1.5 < \leq 3F$	Mixed Tide Tends to Single
$F > 3$	Single Ebb and Flow

3.2.4 River water discharge

River discharge data for 2024 were obtained from the Global Flood Awareness System (GloFAS), a distributed hydrological modelling system developed through collaboration between the European Commission and the ECMWF to monitor and predict flooding in major rivers worldwide. The dataset was provided in the NetCDF format, opened using ODV, and converted into. txt files were used for further processing. Seasonal averages for April and September 2024 were then calculated and used as inputs for hydrodynamic simulations in MIKE 21.

3.3 Nutrient distribution model

Numerical simulations were conducted using the MIKE 21 Flexible Mesh (FM) Integrated Model developed by the DHI. This two-dimensional (2D) model was selected because of its ability to capture the spatial and temporal dynamics of coastal and marine environments with high accuracy. The FM approach enables a detailed representation of the model domain by following the coastline geometry, bathymetry, and other complex features. The computational domain was discretized using an unstructured triangular mesh, with spatial refinement applied in nearshore areas and around river mouths influenced by watershed inputs, whereas coarser elements were used offshore.

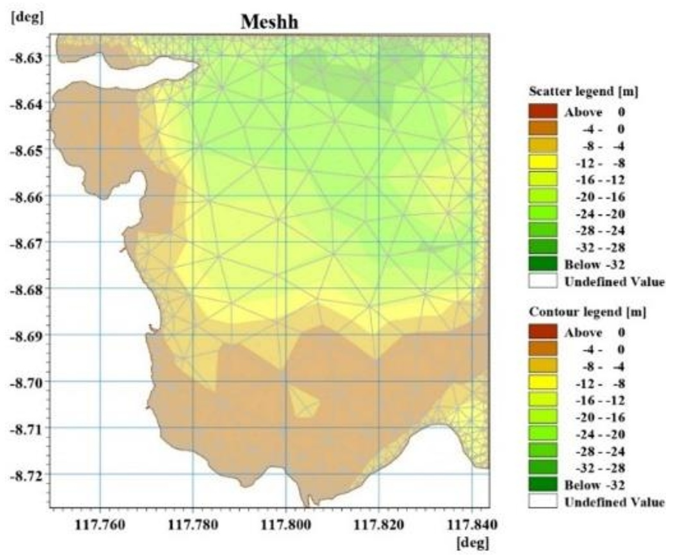

Fig. 5. Mesh domain model.

The simulations were performed for two periods, April 1–30, 2024 and September 1–30, 2024, using a fixed time step interval of 3600 s and a total of 720 time steps for each simulation (Appendix 4). Hydrodynamic initial conditions were defined as a constant water level of 0.0 m, while tidal forcing at the open boundary was derived from the Calabai tidal station and wind forcing was applied using ECMWF datasets for April and September 2024. Bottom friction was represented using a constant Manning number of 32 $m^{1/3}$ s^{-1}, and horizontal turbulence was parameterized using the Smagorinsky formulation with a constant eddy viscosity of 0.28 m^2 s^{-1}, following default MIKE 21 settings (**Table 3**).

Table 3. Model scenario.

Module	Parameter	*Value*
	Specification file	Model Sebaran Nutrien Teluk Saleh.mfm
	Simulation period	1 April 2024 - 30 April 2024 September 2024 - 30 September 2024
	No. of time steps	720, 2 Model
	Time steps interval	*3600s*
	Module Selection	*Hydrodynamics* (HD) Ecolab
HD	*Flood and dry*	*Standard flood and dry*
	Initial conditions	Constant 0.0 m
	Wind forcing	AnginApril.dfs0 AnginSeptember.dfs0
	Wave radiation	(-)
	Eddy viscosity	*Smagorinsky formulation, Constant 0.28 m2/s*
	Bed resistance	*Manning number, Constant 32 m1/s*
Ecolab	*Initial conditions*	(0) Constant
	Boundaries condition	Constant
	Result files	HD.dfsu Ecolab.dfsu
	Simulation time	*About 5 hours*
	PC specification	(-)

The model integrates two primary modules: the Hydrodynamic (HD) module and the ecolabTM module. The HD module simulates current circulation and tidal-induced water-level variations, providing a basis for understanding water mass transport and nutrient dispersion across the study area. The simulations incorporated multiple tidal phases and wind forcing to capture the influence of hydrodynamic drivers on pollutant transport. River discharge from the Bera Watershed was imposed at the Brang Bera, Brang Maronge, and Brang Kolong river mouths using the seasonal average values for April and September 2024 (**Table 4**).

Table 4. River discharge.

River	Time	Discharge (m^3/s)
Brang Maronge	Apr-24	0.4375
	Sep-24	0.4688
Brang Bera	Apr-24	3.75
	Sep-24	2.1875
Brang Kolong	Apr-24	0.5623
	Sep-24	0.6765

The Ecolab module was used to simulate water quality parameters, including dissolved oxygen (DO), nitrate (NO_3), ammonia (NH_4), and phosphate (PO_4). The initial and boundary concentrations for all nutrients were specified as constant values based on in situ measurements collected in 2024, with river boundary concentrations representing land-derived inputs and open boundary values representing offshore background conditions (**Table 5**).

Table 5. Nutrient concentration data.

River Basin	Time	DO	NO_3	PO_4	NH_4
Brang Bera	Apr-24	8.41	0.5	0.145	0.015
	Sep-24	7.97	0.5	0.058	0.013
Brang Maronge	Apr-24	7.81	0.5	0.073	0.009
	Sep-24	7.43	0.5	0.006	0.017
Brang Kolong	Apr-24	7.36	0.6	0.192	0.009
	Sep-24	7.30	0.5	0.188	0.030

This module accounts for key biogeochemical processes, such as nitrification, denitrification, organic matter remineralization, and interactions with aquatic biota [16]. Owing to limited temporal nutrient observations, no extensive parameter calibration was performed, and the reaction parameters followed the default Ecolab coastal water configuration. The integration of the HD and Ecolab modules provides a comprehensive framework for assessing nutrient transport, transformation, and potential eutrophication, thereby supporting evidence-based coastal and marine management. The general equations used in the hydrodynamic and ecolabic modules to describe the hydrodynamic processes and solute transport are as follows:

$$\frac{\partial \eta}{\partial t} + \frac{\partial (hu)}{\partial x} + \frac{\partial (hv)}{\partial y} = 0 \tag{2}$$

$$\frac{\partial (hu)}{\partial t} + \frac{\partial (hu^2)}{\partial x} + \frac{\partial (huv)}{\partial y} = -gh\frac{\partial \eta}{\partial x} + Fx \tag{3}$$

$$\frac{\partial (hu)}{\partial t} + \frac{\partial (hu^2)}{\partial x} + \frac{\partial (huv)}{\partial y} = -gh\frac{\partial \eta}{\partial x} + Fy \tag{4}$$

η : Water surface elevation (m).
$h = \eta + d$: Total water depth (m)
u, v : Directional current speed$x$and (m/s)y
g : Acceleration of gravity
Fx, Fy : External forces (wind, Coriolis force, and friction)

$$\frac{\partial C}{\partial t} + u\frac{\partial C}{\partial x} + v\frac{\partial C}{\partial y} = D_x\frac{\partial^2 C}{\partial x^2} + D_y\frac{\partial^2 C}{\partial y^2} + R(C) \tag{5}$$

C : Concentration of dissolved substances (mg/L)
t : Time (s)
u, v : Current velocity component (m/s) of HD module
D_x, D_y: Horizontal dispersion coefficient (m^2/s)
$R(C)$: Reaction rate (mg/L/s) depending on the type of pollutant

3.4 Model scenario

The model was simulated for a 30-day period covering two representative seasons: April 2024 (Transition Season I) and September 2024 (Transition Season II). Four tidal phases were analyzed: approaching low tide, lowest tide, approaching high tide, and highest tide. A 6-hour spin-up period (21,600 s) using a slow-start scheme was applied to stabilize the initial conditions. The model resolved coupled hydrodynamic and nutrient transport processes using the Hydrodynamic (HD) and Ecolab modules, with tidal forcing prescribed from the Calabai station (BIG) and wind forcing from the ECMWF data to simulate circulation patterns and nutrient dynamics.

3.5 Model validation and calibration

The numerical model was calibrated and validated in two stages, focusing primarily on the hydrodynamic component (HD), as it controls nutrient advection and dispersion. Hydrodynamic simulations were validated against observed tidal elevations from the Calabai station (BIG) and current data from the Copernicus Marine Service using statistical indicators, including the Root Mean Square Error (RMSE), standard deviation, and correlation coefficient, to assess accuracy, variability, and phase agreement [17]. Model skill was further evaluated using Taylor diagrams, which provide an integrated representation of these statistical metrics [18]. Validation of the Ecolab nutrient module (NO_3, NH_4, and PO_4) was constrained by limited field observations available only for April and September 2024; therefore, no extensive calibration of biogeochemical reaction parameters was performed. Nutrient simulations relied on measured concentrations as initial and boundary conditions, whereas biogeochemical processes followed the default MIKE 21 Ecolab coastal water parameterization. Model performance for nutrient distribution was assessed qualitatively by comparing simulated spatial patterns and concentration ranges in situ, highlighting the need for higher-frequency nutrient monitoring in future studies.

$$RMSE = \sqrt{\frac{1}{3}\sum(Y_t - Y_{t+1})^2} \quad (6)$$

$Y_t$is the measurement data; in this case, the tidal data from the BIG station. is the model data, n is the number of measurement data.$Y_t Y_{t+1}$

$$STD = \sqrt{\sum_{i=1}^{N} \frac{(x_1 - x)}{N-1}} \quad (7)$$

$STD$is the standard deviation of the variable [19]. In this case, the tide at the BIG station.x x_i

$$R = \frac{\frac{1}{N}\sum_{i=1}^{N}(f_n - \bar{f})(r_n - \bar{r})}{\sigma_f \sigma_r} \quad (8)$$

$R$is the correlation coefficient, is the mean value, and and are the standard deviations of and respectively [18].

The RMSE assessment criteria refer to [20], which classifies results as Very Good if the value is between 0 and 0.5, good for a value of 0.5 to 0.6, fair in the range of 0.6 to 0.7, and poor if it exceeds 0.7. Meanwhile, according to [21] and [22], the RMSE value is considered low if it is less than half the standard deviation of the observation data.

4 Results and discussion

4.1 Validation of model results with field data

Model validation for tidal dynamics was performed by comparing simulated sea-level elevations with observations from the Calabai tidal station (BIG) for April and September 2024. The model reproduced the observed tidal patterns well, as shown in **Fig. 6** and **Fig. 7**, with low discrepancies quantified using the Root Mean Square Error (RMSE). Admiralty harmonic analysis yielded Formzahl values of 1.3329 in April and 1.2215 in September, indicating a mixed tide with a predominantly diurnal character [15], which is consistent with the observed tidal amplitude variations influenced by both diurnal and semidiurnal constituents. Minor deviations between simulated and observed tides are likely related to model resolution limitations and local environmental variability.

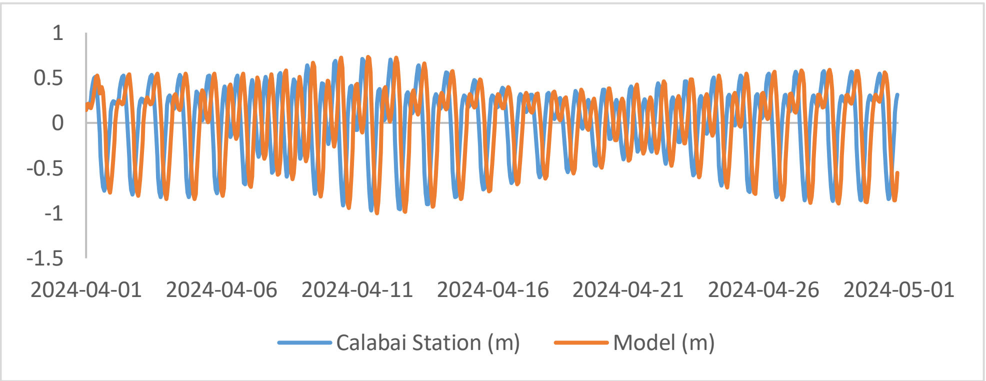

Fig. 6. Comparison of tides in April 2024.

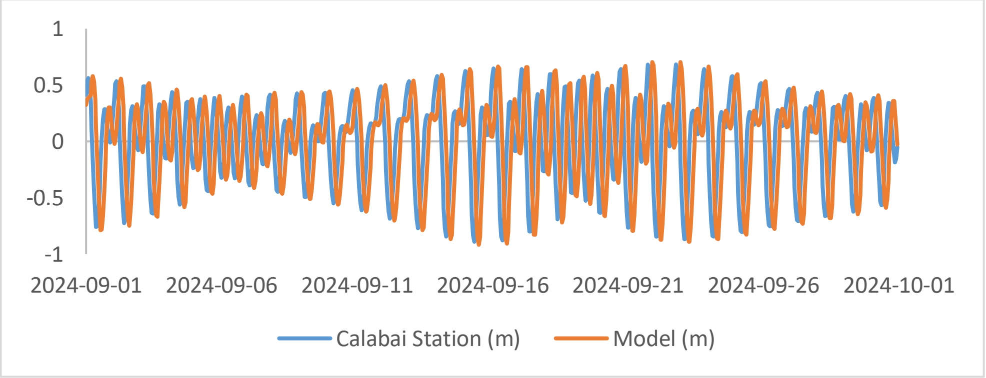

Fig. 7. Comparison of tides in September 2024.

Minor phase differences between observed and simulated tidal elevations are a common feature in hydrodynamic modelling and have been widely reported in coastal and estuarine studies [23, 24]. Such phase lags typically result from the combined effects of grid resolution, boundary forcing, and wave propagation [23]. In this study, the observed phase delays were small and temporally inconsistent, indicating that the dominant diurnal and semidiurnal tidal constituents were well represented, and that the tidal cycles remained well aligned. These minor discrepancies are therefore considered acceptable and do not compromise the ability of the model to simulate hydrodynamic conditions relevant to nutrient transport in Saleh Bay.

Table 6. Tidal model validation results.

Month	RMSE	R	STD
April	0.2296	0.9791	1,1241
September	0.1943	0.9850	1,1231

Based on the results in **Table 6**, the criteria from [19] indicate that the RMSE values for both months are categorized as Very Good because they are below 0.5. Furthermore, according to [21] and [22], the RMSE value is considered low if it is less than half the standard deviation of observations. The RMSE values for April and September also satisfied these criteria.

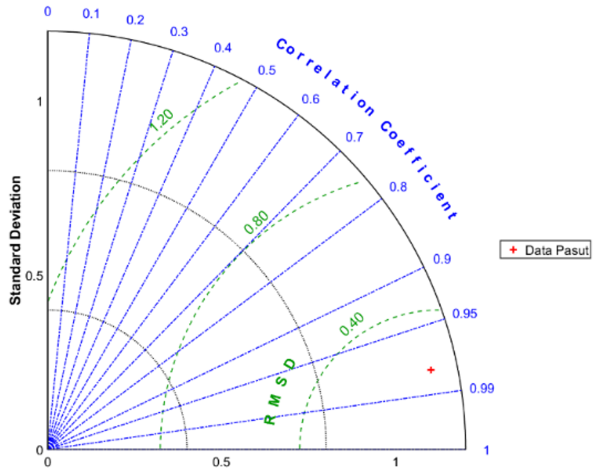

Fig. 8. Taylor diagram of the tides in April 2024.

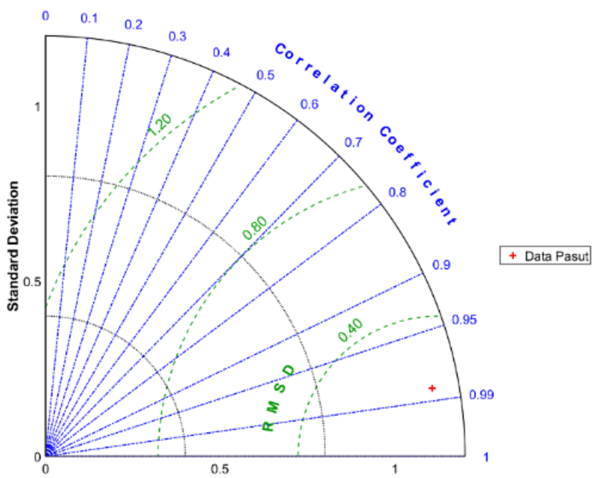

Fig. 9. Taylor diagram of the tides in September 2024.

Fig. 8 and **Fig. 9** show the Taylor Diagram as the result of the tidal model validation against observation data from Calabai Station in Saleh Bay for April and September 2024. This diagram represents the relationship between STD, R, and RMSE, which are commonly used in numerical model evaluation [18].

The model performance was evaluated using both scatter plots and Taylor diagrams, which were constructed from the same paired datasets of the simulated and observed current velocities. The zonal (u) and meridional (v) velocity components extracted from MIKE 21 simulations were directly matched in time and space with the corresponding Copernicus Marine Service data for April 1–30, 2024 and September 1–30, 2024.

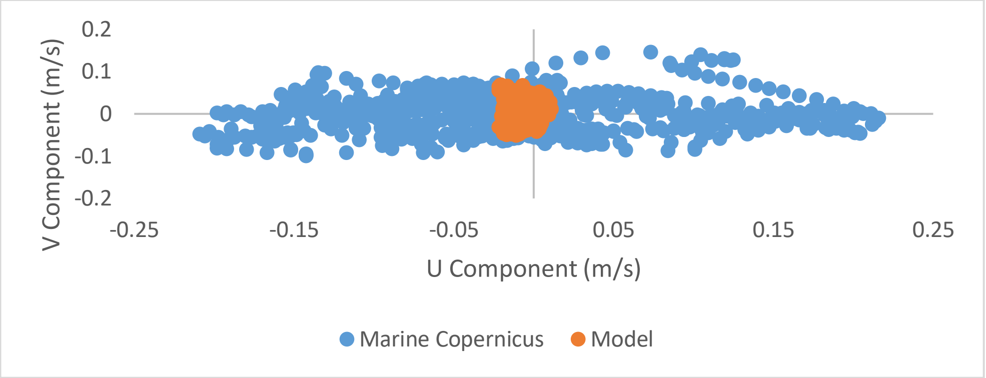

Fig. 10. Results of current speed comparison in April 2024.

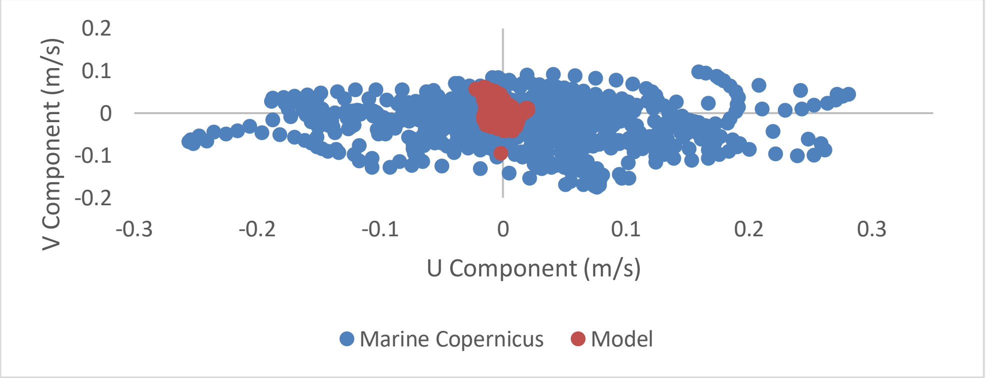

Fig. 11. Current speed comparison results in September 2024.

Scatter plots (**Fig. 10** and **Fig. 11**) and Taylor diagrams (**Fig. 12** and **Fig. 13**), derived from the same paired datasets, consistently demonstrate excellent agreement between the modeled and observed current components. The validation results (**Table 7**) showed very low RMSE values of 0.0316 in April and 0.0340 in September, with identical standard deviations of 1.1142 and extremely high correlation coefficients (R = 0.9996 and 0.9900, respectively). These statistics indicate minimal deviation between simulations and observations, and confirm that the MIKE 21 model reliably reproduces current patterns in Saleh Bay with high accuracy and consistency.

Table 7. Model flow validation results.

Month	RMSE	R	STD
April	0.0316	0.9996	1,1142
September	0.0340	0.9900	1,1142

Fig. 12 and **Fig. 13** present Taylor diagrams summarizing the performance of the MIKE 21 current simulations against the Copernicus Marine Service data for April and September 2024. Both periods exhibited correlation coefficients exceeding 0.99, low RMSE values (0.0316–0.0340 m/s), and comparable standard deviations, indicating excellent agreement between the modeled and observed current components. According to the performance classification of [18], the model achieved a “Very Good” rating for both months, confirming that the MIKE 21 model reliably and accurately represents the hydrodynamic conditions in Saleh Bay.

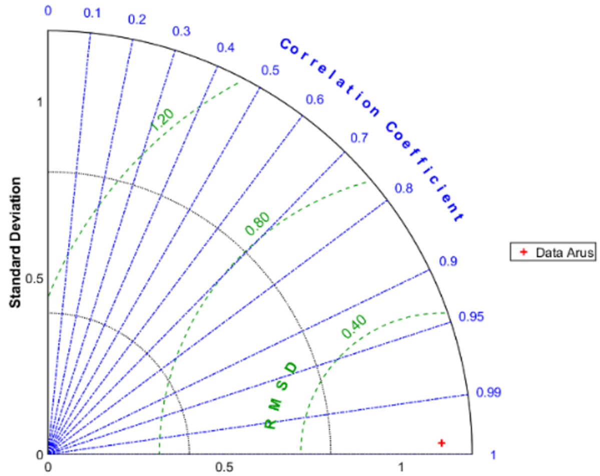

Fig. 12. Taylor diagram of current in April 2024.

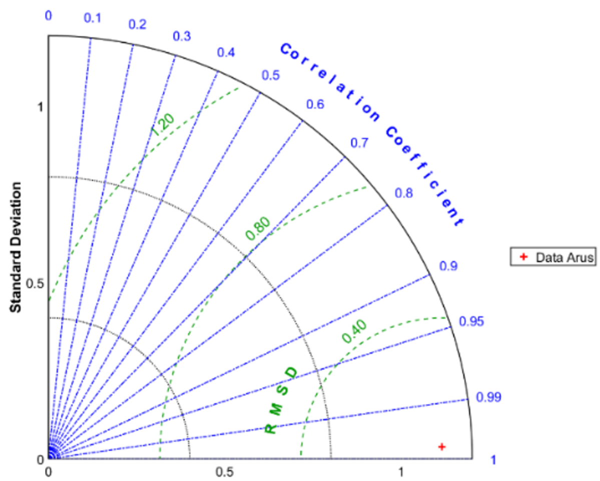

Fig. 13. Taylor diagram of current in September 2024.

4.2 Flow pattern of model results in Saleh Bay

The simulation results show the spatial distribution of currents in Saleh Bay during April 2024 across the four tidal phases (**Fig. 14**). During the approaching low tide, the dominant current flowed out of the bay through the southern boundary, with circulation patterns generally parallel to the shoreline in the western and southwestern regions. Current velocities in this phase range from 0.03–0.27 m/s, with the strongest values observed in the northwestern part of the bay. At low tide, the current direction remained relatively consistent, although the velocity decreased, particularly along the western and southwestern coasts, ranging from 0.03–0.21 m/s. When the tide begins to rise, currents begin entering the bay from the southeast and move northwestward across the central to northern areas, with velocities locally increasing up to 0.27 m/s in the northern region. At the highest tide, the current pattern continued to show inflow from the open sea toward the bay, although with reduced intensity, with velocities ranging between 0.03–0.15 m/s. These results indicate that tidal forcing plays a major role in shaping circulation patterns, with ebb phases characterized by dominant outflow and flood phases characterized by dominant inflow.

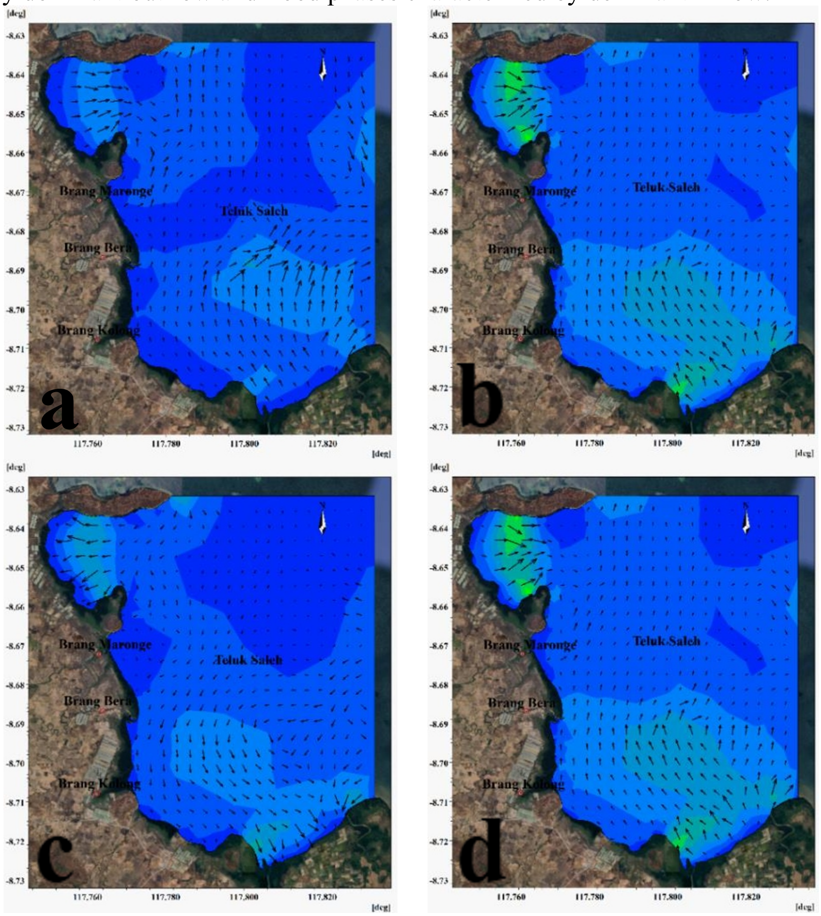

Fig. 14. Current speed in Saleh Bay in April 2024 at (a) the lowest ebb, (b) the lowest ebb, (c) the highest tide and (d) the highest tide.

The simulation results revealed the current patterns in Saleh Bay during September 2024 across the four tidal phases (**Fig. 15**). During the approaching low tide, currents predominantly flowed out of the bay toward the southeast, with circulation patterns aligned parallel to the northern and northeastern coastlines. Velocities range from 0.03–0.24 m/s, with the strongest flows occurring in the northern and central parts of the bay. At low tide, the overall current direction remains relatively unchanged, although the velocities decrease along the western and eastern coasts, ranging from 0.03–0.18 m/s. As the tide rises, currents enter the bay from the southeast and move northwestward across the central region, forming a more organized circulation pattern, with velocities reaching up to 0.24 m/s. At the highest tide, inflow from the open sea persists but with reduced intensity, ranging from 0.03–0.12 m/s. These results highlight the consistent tidal control on circulation dynamics, with ebb phases dominated by southeastward outflow and flood phases dominated by organized inflow from the southeast.

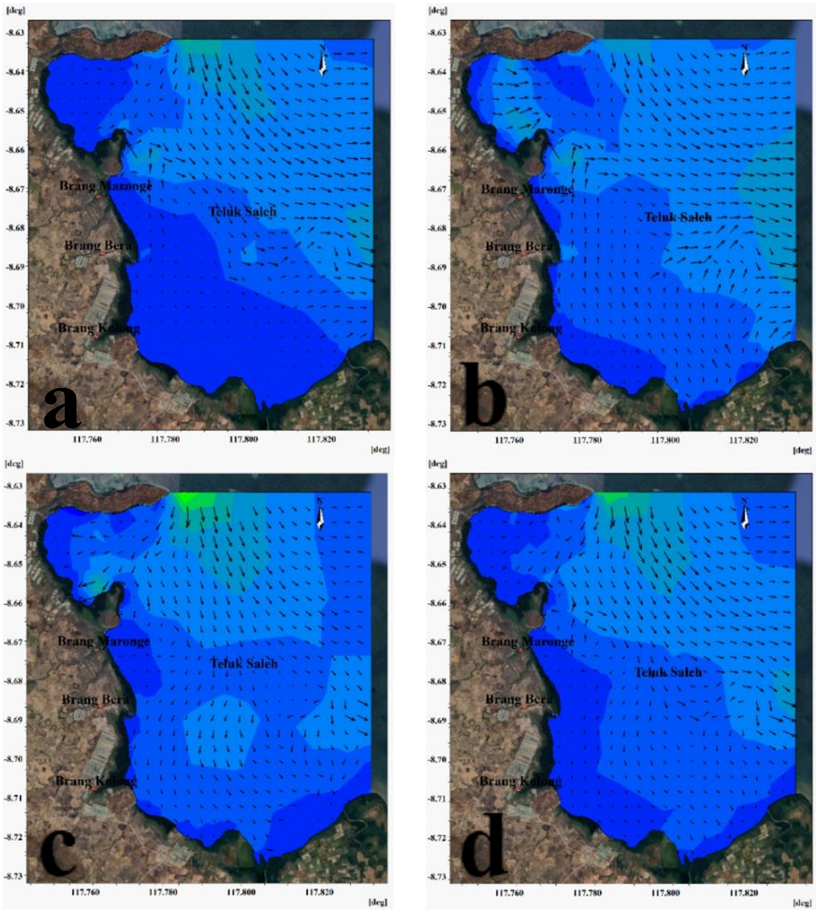

Fig. 15. Current speed in Saleh Bay in September 2024 at (a) the lowest ebb, (b) the lowest ebb, (c) the highest tide and (d) the highest tide.

The variations in current patterns and velocities in Saleh Bay confirm that the water circulation in this semi-enclosed system is primarily governed by tidal forcing rather than seasonal influences. In both April and September 2024, the circulation patterns exhibited a strong correspondence with tidal phases, with currents consistently flowing into and out of the bay in response to sea level fluctuations. This finding is consistent with [25], who emphasized that tidal characteristics and bottom morphology are the dominant controls on the circulation in semi-enclosed coastal waters. These factors strongly influence the water mass exchange, circulation efficiency, and spatial distribution of materials within the bay.

4.3 Nutrient distribution patterns based on model results in Saleh Bay

4.3.1 DO distribution pattern of model results

The modeling results indicate the spatial distribution of dissolved oxygen (DO) concentrations in Saleh Bay during April 2024 across the four tidal phases (**Fig. 16**). In the period preceding low tide, high DO concentrations (>6 mg/L) dominated the central and coastal zones of the bay, whereas the southern area exhibited relatively low levels, suggesting limited oxygen exchange beyond the model domain [25]. At the lowest tide, DO concentrations declined and areas with values below 3 mg/L expanded, particularly along the coastline, likely driven by water mass stagnation and organic matter decomposition [26]. During the rising tide, the inflow of seawater transported oxygen into the southern bay, elevating DO levels in this region. At high tide, enhanced mixing resulted in a more uniform distribution, with concentrations generally exceeding 4 mg/L throughout the study area.

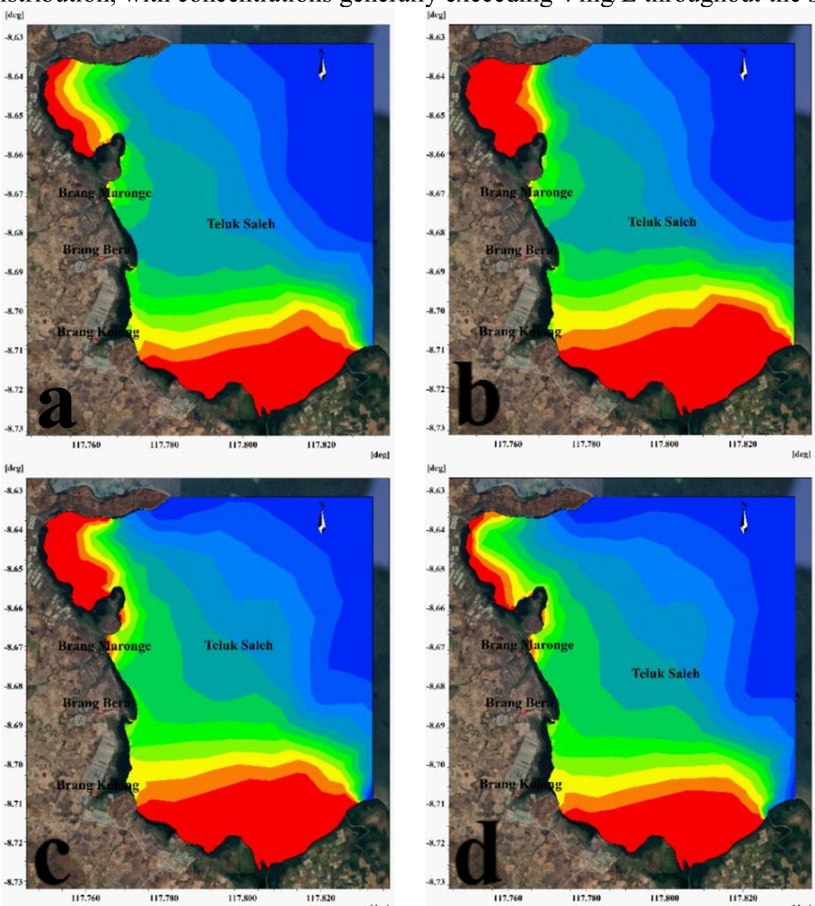

Fig. 16. DO pattern in Saleh Bay in April 2024 at (a) the lowest ebb, (b) the lowest ebb, (c) the highest tide and (d) the highest tide.

The modelling results illustrate the spatial distribution of dissolved oxygen (DO) in Saleh Bay during September 2024 across the four tidal phases (**Fig. 17**). In the period preceding the low tide, relatively high DO concentrations (>6 mg/L) dominated the central and coastal regions, although the southern shallow areas began to exhibit lower values, suggesting organic matter accumulation [27]. At the lowest tide, the zones with DO levels below 3 mg/L expanded considerably, particularly along the western coastline. During the rising tide, the inflowing seawater introduced additional oxygen, leading to localized increases in DO, albeit with an uneven distribution across the bay. At high tide, enhanced mixing produced a more homogeneous pattern, with concentrations generally exceeding 4 mg/L throughout most of the areas.

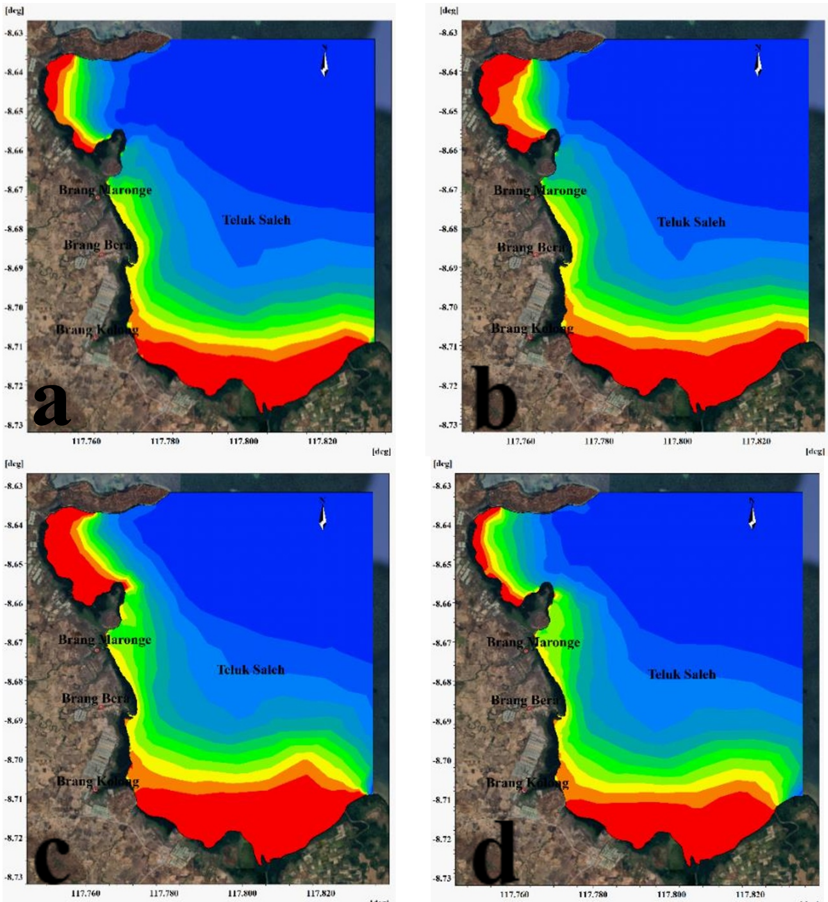

Fig. 17. DO pattern in Saleh Bay in September 2024 at (a) the lowest ebb, (b) the lowest ebb, (c) the highest tide and (d) the highest tide.

The spatial distribution of dissolved oxygen and nutrients in Saleh Bay is strongly controlled by tidal-driven hydrodynamics, which regulate water exchange, mixing intensity, and residence time in this semi-enclosed system [3, 14]. During the low tide and ebb phases, weakened circulation promotes nutrient accumulation in nearshore areas, particularly near river mouths and along the western and southwestern coasts, where organic matter inputs from agriculture, domestic wastewater, and aquaculture increase oxygen consumption and lead to localized hypoxic conditions (DO < 3 mg/L) [10, 24]. In contrast, rising and high tide phases enhance tidal mixing and facilitate the intrusion of oxygen-rich offshore waters, resulting in more homogeneous DO distributions and the partial dilution of accumulated nutrients [14, 24]. Differences in nutrient behavior reflect their biogeochemical characteristics: low NH_4 concentrations indicate efficient nitrification under predominantly oxic and well-mixed conditions [28, 29], whereas NO_3 shows higher spatial variability owing to strong watershed-derived inputs and accumulation during weak tidal exchange [5, 10]. PO_4 exhibits more localized enrichment, suggesting strong control by sediment interactions and rapid biological uptake that limit its horizontal dispersion even under high tidal mixing [30, 31]. Overall, tidal mixing acts as a key regulatory mechanism that can either intensify oxygen depletion and nutrient retention under low mixing conditions or mitigate eutrophication through dilution and redistribution during stronger tidal phases [14, 32].

4.3.2 NH_4 distribution pattern from model results

The modeling results illustrate the spatial distribution of ammonia (NH_3) concentrations in Saleh Bay during April 2024 across the four tidal phases (**Fig. 18**). Overall, NH_4 levels were categorized as very low (<0.003 mg/L), as reflected by the predominance of dark to light blue shading across all phases. These values suggest that NH_4 pollution in Saleh Bay during April was minimal and remained below the seawater quality threshold for marine biota. Slight increases in NH_4 concentrations (0.003–0.005 mg/L) were observed in localized coastal areas of the east and northwest during ebb and high tide, likely linked to anthropogenic inputs or remobilization of ammonia from shallow sediments under varying hydrodynamic conditions [32].

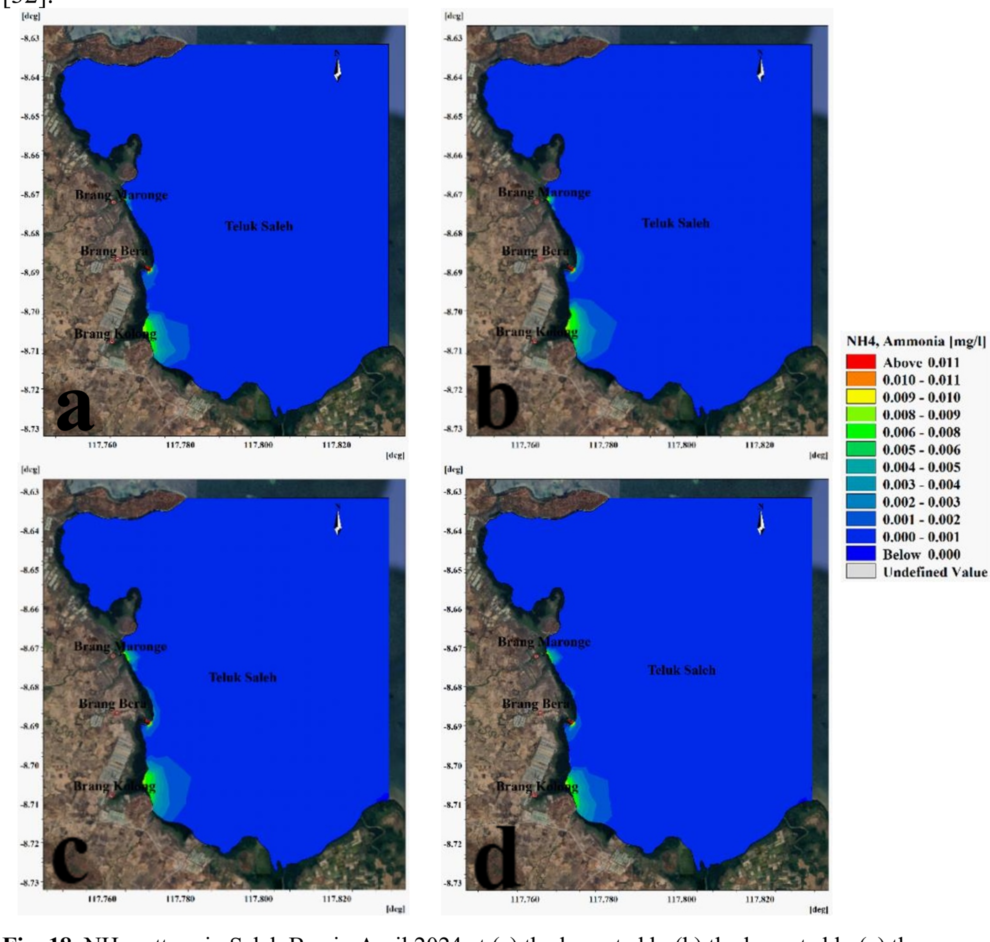

Fig. 18. NH_4 pattern in Saleh Bay in April 2024 at (a) the lowest ebb, (b) the lowest ebb, (c) the highest tide and (d) the highest tide.

The modelling results for September 2024 (**Fig. 19**) show a distribution pattern of NH_4 similar to that observed in April. Across all tidal phases, NH_4 concentrations remained very low (<0.003 mg/L), confirming that Saleh Bay waters are generally not under significant ammonia pollution pressure. Nonetheless, localized increases (0.003–0.005 mg/L) were more noticeable in September, particularly along the eastern and northwestern coasts. These increases may be linked to enhanced land runoff during the rainy season or the accumulation of organic matter from terrestrial nutrient inputs [34]. Importantly, these elevated concentrations were confined to nearshore zones and did not extend into the central bay, suggesting that mixing and circulation processes remained effective in diluting the ammonia levels.

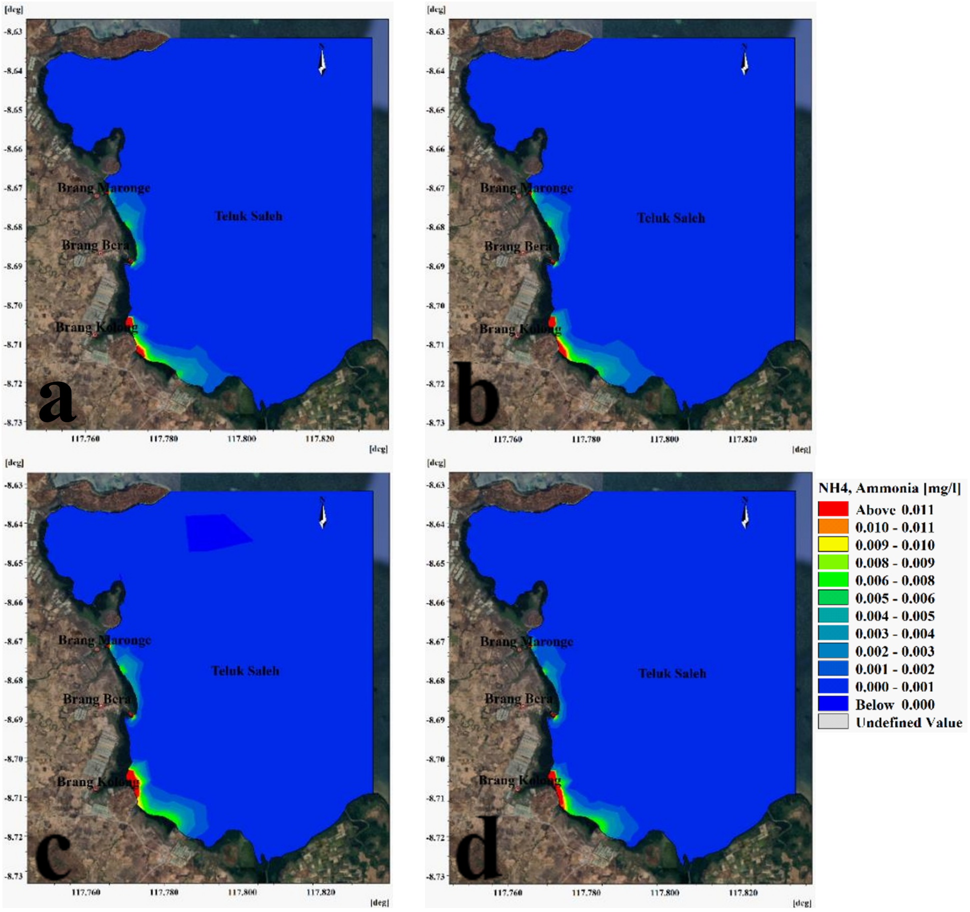

Fig. 19. NH_4 pattern in Saleh Bay in September 2024 at (a) the lowest ebb, (b) the lowest ebb, (c) the highest tide and (d) the highest tide.

Differences in NH_4 distribution patterns between April and September 2024 indicate episodic land-based inputs and possible sediment remobilization in shallow coastal zones [35]. During the lowest tide and the transition toward high tide, NH_4 concentrations remained relatively low and were primarily concentrated along the southwest coast, likely influenced by anthropogenic activities, such as mariculture and land runoff [36]. During the highest tide phase, enhanced tidal mixing resulted in a slightly broader but still localized distribution, reflecting the role of tidal circulation in horizontally redistributing NH_4 within the bay.

The consistently low NH_4 concentrations suggest efficient nitrogen transformation under predominantly oxic conditions. Regular tidal mixing enhances oxygen availability and promotes rapid nitrification, thereby limiting NH_4 accumulation despite ongoing anthropogenic inputs from aquaculture and terrestrial runoff [28, 29]. Localized NH_4 increases during low tide, further emphasizing the influence of reduced mixing and sediment–water interactions in coastal areas [36, 37]. These results highlight the dominant role of tidal dynamics in regulating the accumulation, transformation, and dispersion of NH_4 in Saleh Bay [7, 14].

4.3.3 NO_3 distribution pattern from model results

The modeling results illustrate the spatial distribution of NO_3 concentrations in Saleh Bay during April 2024 across four tidal phases, as presented in **Fig. 20** the approach to the lowest tide, lowest tide, approach to the highest tide, and highest tide. Overall, NO_3 concentrations were categorized as low to moderate (<0.03 mg/L), indicated by the predominance of dark blue to light green shades across most of the bay. Nevertheless, localized areas with higher concentrations (>0.03–0.055 mg/L) were detected along the southwest and southern coasts, particularly during the lowest and highest tidal phases. This spatial pattern suggests potential nitrogen inputs from terrestrial sources, such as river discharge or surface runoff, transporting fertilizers and domestic waste. The accumulation of NO_3 in these areas is likely intensified during tidal transitions when the water mass exchange with the open sea is constrained, leading to nutrient retention in coastal zones [14].

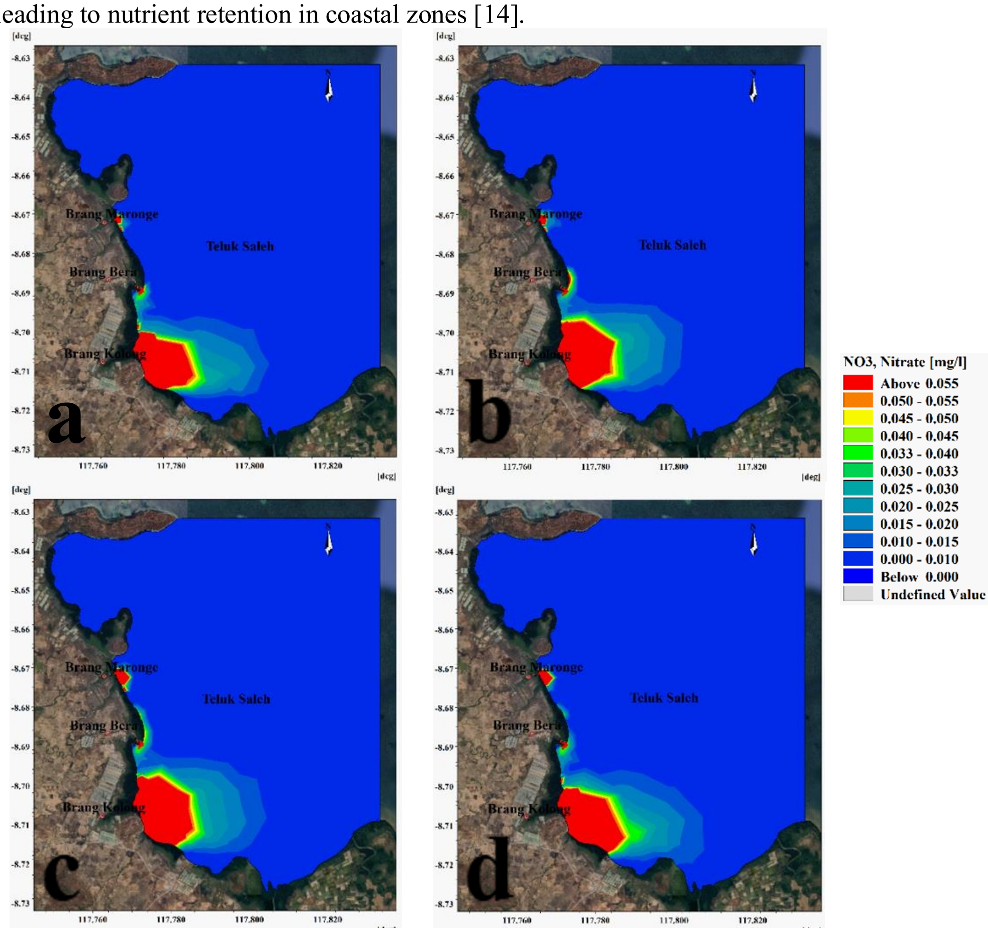

Fig. 20. NO_3 pattern in Saleh Bay in April 2024 at (a) the lowest ebb, (b) the lowest ebb, (c) the highest tide and (d) the highest tide.

The modeling results for September 2024 show a comparable distribution pattern, as presented in **Fig. 21**, covering the phases approaching the lowest tide, lowest tide, approach to the highest tide, and highest tide. Overall, NO_3 concentrations remained low (<0.03 mg/L); however, localized increases (0.03–0.045 mg/L) were observed along the southwest and northeast coasts. These elevated concentrations were most prominent during the lowest tide and approached the highest tide, which may be attributed to the accumulation of land-based runoff during the wet season. Compared to April, the zones of elevated concentrations appeared more restricted but exhibited spatial shifts, reflecting seasonal differences in nitrogen inputs and the influence of local circulation dynamics on nutrient distribution [4].

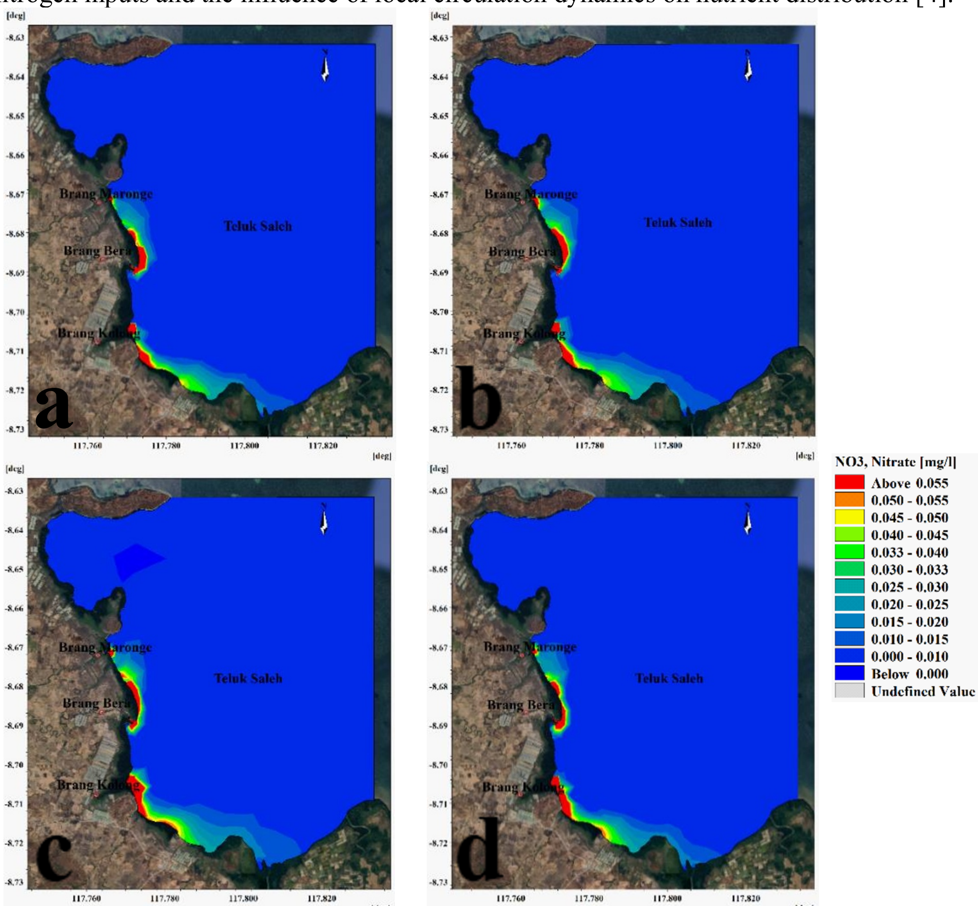

Fig. 21. NO_3 pattern in Saleh Bay in September 2024 at (a) the lowest ebb, (b) the lowest ebb, (c) the highest tide and (d) the highest tide.

Elevated NO_3 concentrations in April indicate episodic nutrient inputs from surface runoff, coastal activities, and possible sediment remobilization, with higher levels observed along the southwestern coast during low to near-high tide phases, likely associated with aquaculture and land-based inputs [28, 37]. Enhanced tidal mixing during high tides promotes a more uniform horizontal distribution, highlighting the role of tidal circulation in nutrient dispersion [7]. In contrast, September shows more spatially restricted and stable NO_3 patterns, with elevated concentrations persisting in nearshore zones during low tide, suggesting seasonal variability in nutrient inputs and sediment-related processes [13]. Overall, NO_3 exhibits higher spatial variability than NH_4 due to its dominance under oxic conditions and strong watershed-derived inputs from the Bera Watershed [5, 28]. Limited water exchange during low tide favors nearshore NO_3 accumulation and increases eutrophication risk [10, 32], whereas flood tides enhance dispersion and partial export toward the central bay, underscoring the key role of tidal dynamics in regulating NO_3 retention and dilution in Saleh Bay [14].

4.3.4 PO_4 distribution pattern from model results

The modelling results indicate the spatial distribution of PO_4 concentrations in Saleh Bay in April 2024 across four tidal phases, as illustrated in **Fig. 22**, approaching low tide, low tide, approaching high tide, and high tide. Overall, PO_4 concentrations were low (<0.010 mg/L), as reflected by the predominance of blue shading across most of the bay. However, localized increases (≥0.014 mg/L) were detected along the southwest and northeast coasts, particularly during the approaching low-tide and high-tide phases. These localized enrichments suggest potential phosphate inputs from land-based runoff or river discharge as well as possible remobilization of shallow sediments during tidal fluctuations [29, 38].

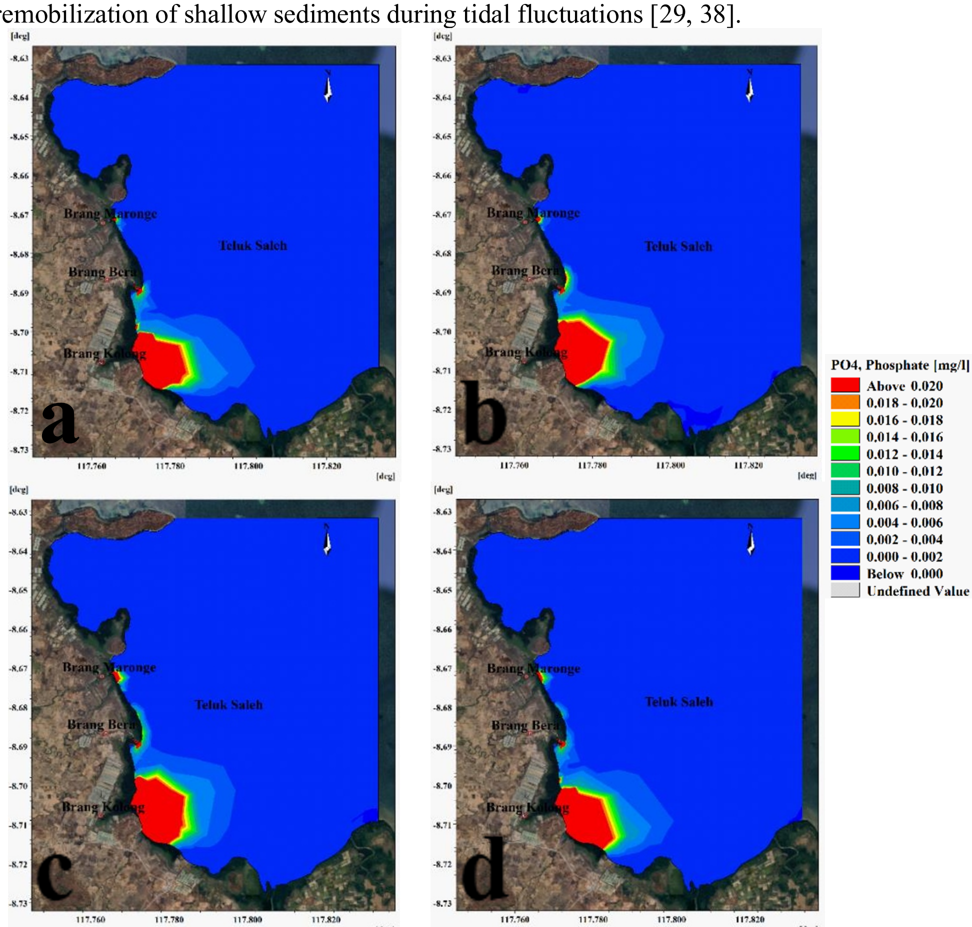

Fig. 22. PO_4 pattern in Saleh Bay in April 2024 at (a) the lowest ebb, (b) the lowest ebb, (c) the highest tide and (d) the highest tide.

The modeling results illustrate the spatial distribution of PO_4 concentrations in Saleh Bay in September 2024 across four tidal phases, as shown in **Fig. 23**, approaching low tide, low tide, approaching high tide, and high tide. The overall distribution pattern was similar to that observed in April, with generally low concentrations (<0.010 mg/L) across most of the bay. Localized increases (≥0.014 mg/L) were detected along the western and southwestern coasts, particularly during the low-tide and high-tide phases. These elevated concentrations may reflect the influence of anthropogenic activities, such as mariculture or domestic runoff, in addition to natural processes, including nutrient resuspension from shallow sediments [37].

This finding further highlights the critical role of tidal dynamics in regulating the horizontal distribution of phosphate in Saleh Bay [14].

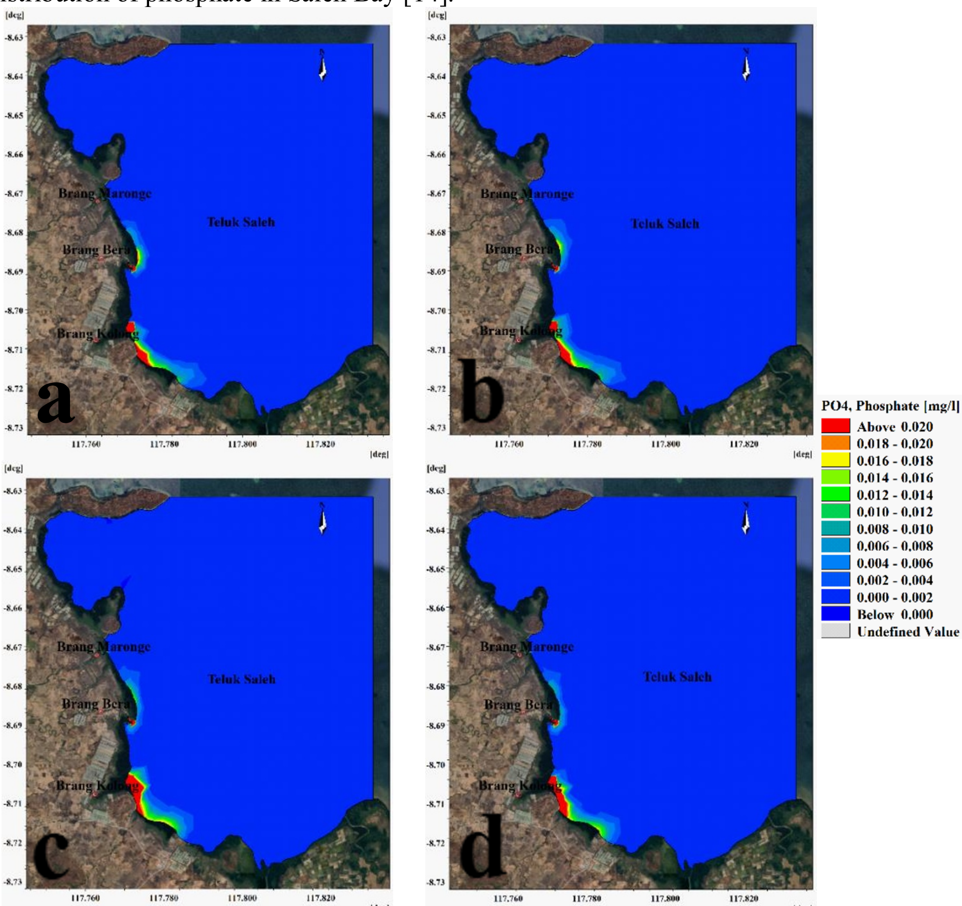

Fig. 23. PO_4 pattern in Saleh Bay in September 2024 at (a) the lowest ebb, (b) the lowest ebb, (c) the highest tide and (d) the highest tide.

The occurrence of locally elevated PO_4 concentrations in April indicates the influence of land-based inputs, such as rainfall-induced runoff, domestic sewage, aquaculture activities, and the remobilization of shallow sediments [28, 38, 39]. Recurring enrichment along the southwest and northeast coasts suggests persistent anthropogenic pressure in these areas [7]. The relatively narrow horizontal distribution during most tidal phases implies that tidal dynamics were not sufficient to disperse PO_4 widely, and that phosphate was rapidly assimilated by phytoplankton or retained through sediment interactions [10, 31].

In September, PO_4 distributions appeared more stable, with elevated concentrations remaining localized in coastal zones, particularly during low and high tides, likely linked to seasonal land runoff and aquaculture inputs [37]. Reduced mixing during low tide enhanced PO retention, whereas increased dispersion during high tide reflected the role of tidal mixing, although the overall spread remained limited. These results confirm that PO dynamics in Saleh Bay are primarily controlled by land-derived inputs and modulated by local circulation and tidal processes [30, 38].

5 Conclusion

The modeling results show that nutrient distributions (NH_4, NO_3, and PO_4) in Saleh Bay are primarily concentrated in nearshore waters, especially around river estuaries connected to the Bera Watershed, highlighting the dominant influence of land-based inputs. NH_4 and PO_4 concentrations were generally low but exhibited localized enrichments exceeding 0.005 mg/L and 0.014 mg/L along the western and southwestern coasts, while NO_3 reached higher levels (>0.055 mg/L) near the southwest coast, reflecting watershed-derived inputs from agricultural runoff and domestic effluents. These spatial patterns indicated that nutrient accumulation is closely linked to estuarine proximity and limited water exchange. The results demonstrate the value of numerical modeling in identifying pollution-prone zones and supporting integrated coastal management. From a management perspective, nutrient load reduction in the Bera Watershed through improved agricultural practices, wastewater treatment, and erosion control, supported by routine monitoring in high-risk coastal areas, is recommended. Despite the limitations related to the absence of in situ nutrient validation and the use of a two-dimensional model, this framework provides a strong basis for future studies employing more intensive observations and three-dimensional ecosystem-coupled models to better assess eutrophication risks in Saleh Bay.

This study was funded by the RIIM G-2/2022, BRIN- Indonesia Endowment Fund for Education Agency [LPDP]. National Research and Innovation Agency [Grant number 82/II.7/HK/2022]; Contract Number: B-1740/II.7.5/FR/11/2022 and B-15177/III.4/KS.00/11/2022. The authors also thank the Research Center for Conservation of Marine and Inland Water Resources, BRIN; Sumbawa Regency Government (PEMDA); and the Department of Marine Science, FPIK, Post-Graduate School IPB University, and Coastal Dynamics Laboratory, Directorate of Laboratory Management Research Facilities.

References

1. I.N. Edrus, S. Arief, I.E. Setyawan, Kondisi kesehatan terumbu karang Teluk Saleh, Sumbawa. J. Penelit. Perikanan Indonesia. **16**, 147 (2010). https://doi.org/10.15578/jppi.16.2.2010.147-161
2. M. Ramdhan, R. Akhwady, T. Arifin, D. Purbani, Yulius, D.G. Pryambodo, R. Rahmania, O. Maftukhaturrizqoh, A. Asyiri, S. Hidayat, A. Ningsih, Sadad, Using neural networks for sustainable land use prediction in Sumbawa Regency, Indonesia Appl. Environ. Res. **46** (2024). https://doi.org/10.35762/AER.2024045
3. R.P. Sari, N.R. Sunarti, A. Walid, Dampak dampak pencemaran Pantai Tapak Paderi Kota Bengkulu akibat sampah terhadap kelestarian laut di Indonesia. TIN: Terapan Inform. Nusantara. **1**, 109 (2020)
4. C. Cahyana, Model sebaran radionuklida antropogenik di laut. J. Teknol. Pengelolaan Limbah. **15**, 17 (2012)
5. S.R. Carpenter, Eutrophication of aquatic ecosystems: bistability and soil phosphorus, Proc. Natl. Acad. Sci. U.S.A. **102**, 10002–10005 (2005). https://doi.org/10.1073/pnas.0503959102
6. S.S. Chen, I.A. Kimirei, C. Yu, Q. Shen, Q. Gao, Assessment of urban river water pollution with urbanization in East Africa. Environ. Sci. Pollut. Res. **29**, 40812 (2022). https://doi.org/10.1007/s11356-021-18082-1
7. V.H. Smith, G.D. Tilman, J.C. Nekola, Eutrophication: impacts of excess nutrient inputs on freshwater, marine, and terrestrial ecosystems. Environ. Pollut. **100**, 179 (1999). https://doi.org/10.1016/S0269-7491(99)00091-3

8. A.R. Adhitia, Deskripsi umum, fenomena menarik dan rencana pengem-bangan di Teluk Saleh dan laut sekitarnya. JOANE**.** **1**, 54 (2023). https://doi.org/10.56855/v1i3.820
9. W.O. Risna, M.S. Safilu, M. Sirih, Analisis tingkat pencemaran perairan Teluk Kendari berdasarkan keanekaragaman gastropoda (Prosobranchia). J. Alumni Pendidik. Biol. **7**, 92 (2022). https://doi.org/10.36709/ampibi.v7i2.24486
10. A.R. Nugroho, R. Akhwady, D. Metakaryanto, F. Yahya, Studi model distribusi pencemaran di Pantai Utara Jawa Tengah menggunakan model MIKE 21 ECOLab. J. Sains Teknol. Lingkungan. **8**, 89 (2016). https://doi.org/10.20885/jstl.vol8.iss2.art3
11. A.M. Rahman, D. Purbani, S.B. Agus, T. Arifin, Y. Yulius, A. Putra, A. Heriati, J. Prihantono, R. Akhwady, A. Sufyan, E. Mustikasari, S.E. Purnamaningtyas, R. Rahmania, M. Ramdhan, A. Ningsih, S. Sadad, D.W.H. Tjahjo, Hydrodynamic modeling of pollutant distributions from the Bera watershed and its impact to the coastal area of Saleh Bay, West Nusa Tenggara, Indonesia. Geographia Technica. **20**, 31 (2025). https://doi.org/10.21163/GT_2025.202.03
12. R. Vaquer-Sunyer, C.M. Duarte, Thresholds of hypoxia for marine biodiversity. Proc. Natl. Acad. Sci. USA. **105**, 15452 (2008). https://doi.org/10.1073/pnas.0803833105
13. S.P. Seitzinger, J.A. Harrison, E. Dumont, A.H.W. Beusen, A.F. Bouwman, Sources and delivery of carbon, nitrogen, and phosphorus to the coastal zone: an overview of Global Nutrient Export from Watersheds (NEWS) models and their application. Global Biogeochem. Cycles. **19** (2006). https://doi.org/10.1029/2005GB002606
14. A. Yulius, A. Heriati, E. Mustikasari, R.I. Zahara, Karakteristik pasang surut dan gelombang di perairan Teluk Saleh, Nusa Tenggara Barat. J. Segara. **13**, 1 (2017), https://doi.org/10.15578/segara.v13i1.6423
15. S. Pond, Introductory dynamical oceanography (Pergamon Press, Oxford, 1983). https://doi.org/10.1016/B978-0-08-057054-9.50007-9
16. J. Prihantono, I.A. Fajrianto, Y.N. Kurniadi, Pemodelan hidrodinamika dan transpor sedimen di sekitar Tanjung Pontang, Kabupaten Serang – Banten. J. Kelaut. Nasional. **13**, 75 (2018). https://doi.org/10.15578/jkn.v1i2.6614
17. T. Chai, R.R. Draxler, Root mean square error (RMSE) or mean absolute error (MAE)? – Arguments against avoiding RMSE in the literature. Geosci. Model Dev. **7**, 1247 (2014). https://doi.org/10.5194/gmd-7-1247-2014
18. K.E. Taylor, Summarizing multiple aspects of model performance in a single diagram. J. Geophys. Res. Atmos. **106**, 7183 (2001). https://doi.org/10.1029/2000JD900719
19. R.E. Thomson, W.J. Emery, Data analysis methods in physical oceanography (Elsevier, Waltham, 2014). https://doi.org/10.1016/B978-0-12-387782-6.00005-3
20. A. Milasari, D.H. Ismunarti, E. Indrayanti, F. Muldiyatno, A. Ismanto, A. Rifai, Model arus permukaan Teluk Lampung pada musim peralihan ii dengan pendekatan hidrodinamika. Bul. Oseanogr. Mar. **10**, 259 (2021). https://doi.org/10.14710/buloma.v10i3.38293
21. D.N. Moriasi, J.G. Arnold, M.W. Van Liew, R.L. Bingner, R.D. Harmel, T.L. Veith, Model evaluation guidelines for systematic quatification of accuracy in watershed simulations. Trans. ASABE. **50**, 885 (2007). https://doi.org/10.13031/2013.23153
22. J.W. Singh, H.V. Knapp, J.G. Arnold, M. Demissie, Hydrological modeling of the iroquois river watershed using HSPF and SWAT. JAWRA J. Am. Water Resour. Assoc. **41**, 343 (2004). https://doi.org/10.1111/j.1752-1688.2005.tb03740.x

23. I.P. Medvedev, E.A. Kulikov, I.V. Fine, Numerical modelling of teh Caspian Sea tides. Ocean Sci. **16**, 209–219 (2020). https://doi.org/10.5194/os-16-209-2020
24. U.J. Wisha, I. Ilham, Velocity components of currents and transport mechanism in teh le Meulee Waters, Weh Island, Indonesia. J. Ilmu Teknol. Kelaut. Trop. **22**, 93–102 (2019). https://doi.org/10.14710/jkt.v22i2.5779
25. H. Effendi, Telaah kualitas air (Kanisius, Yogyakarta, 2003)
26. I.A. Soegianto, Ekologi perairan tawar (Airlangga Univ. Press, Surabaya, 2019
27. S. Jubaedah, S.Y. Wulandari, M. Zainuri, L. Maslukah, D.H. Ismunarti, Studi Kandungan bahan organik di perairan muara Sungai Jajar, Kabupaten Demak, Jawa Tengah. Indones. J. Oceanogr. **3**, 230 (2020). https://doi.org/10.14710/ijoce.v3i3.11442
28. J.N. Galloway, J.D. Aber, J.W. Erisman, S.P. Seitzinger, R.W. Howarth, E.B. Cowling, B.J. Cosby, The nitrogen cascade. BioScience**. 53**, 341 (2003). https://doi.org/10.1641/0006-3568(2003)053[0341:TNC]2.0.CO;2
29. R.W. Howarth, R. Marino, Nitrogen as the limiting nutrient for eutrophication in coastal marine ecosystems: Evolving views over three decades. Limnol. Oceanogr. **51**, 364 (2006). https://doi.org/10.4319/lo.2006.51.1_part_2.0364
30. C.R. Benitez-Nelson, The biogeochemical cycling of phosphorus in marine system. Earth-Sci. Rev. **51**, 109 (2000). https://doi.org/10.1016/S0012-8252(00)00018-0
31. J.J. Elser, M.E.S. Bracken, E.E. Cleland, D.S. Gruner, W.S. Harpole, H. Hillebrand, J.T. Ngai, E.W. Seabloom, J.B. Shurin, J.E. Smith, Global analysis of nitrogen and phosphorus limitation of primary producers in freshwater, marine and terrestrial ecosystems. Ecol. Lett. **10**, 1135 (2007). https://doi.org/10.1111/j.1461-0248.2007.01113.x
32. B.A. Stauffer, A. Schnetzer, A.G. Gellene, C. Oberg, G.S. Sukhatme, D.A. Caron, Effects of an acute hypoxic event on microplankton community structure in a coastal harbor of Southern California. Estuaries Coasts. **6**, 135 (2013). https://doi.org/10.1007/s12237-012-9551-6
33. T. Prartono, T. Hasena, Kinetic study of phosphor dan nitrogen compounds from sedimentary re-suspension. E-J. Ilmu Teknol. Kelautan Tropis**. 1**, 1 (2009). https://doi.org/10.28930/jitkt.v1i1.7933
34. A. Muadifah, Pengendalian pencemaran lingkungan (MNC Publishing, Malang, 2019)
35. E.D. Pertiwi, S. Widada, B. Rochaddi, H. Hariyadi, W. Atmodjo, M. Yusuf, A. Rifai, Interpretasi litologi dasar laut pada muara sungai dan lepas pantai berdasarkan analisa shallow seismic di Perairan Sumbawa, Nusa Tenggara Barat. Indones. J. Oceanogr. **2**, 341 (2019). https://doi.org/10.14710/ijoce.v2i4.8612
36. K. Mustiawan, S.Y. Wulandari, E. Indrayanti, Distribusi konsentrasi nitrogen anorganik terlarut pada saat pasang dan surut di Muara Sungai Perancak dan Industri Pelabuhan Perikanan Pengambengan Bali. J. Oceanogr. **3**, 438 (2014)
37. M.S. Islam, M. Tanaka, Impacts of pollution on coastal and marine ecosystems including coastal and marine fisheries and approach for management: a review and synthesis. Mar. Pollut. Bull. **48**, 624 (2004). https://doi.org/10.1016/j.marpolbul.2003.12.004
38. D.L. Correll, The role of phosphorus in the eutrophication of receiving waters: a review. J. Environ. Qual. **27**, 261 (1998). https://doi.org/10.2134/jeq1998.00472425002700020004x
39. S.W. Nixon, Coastal marine eutrophication: A definition, social causes, and future concerns. Ophelia. **41**, 199 (1995). https://doi.org/10.1080/00785236.1995.10422044